

Quasi-phase-matched optical parametric oscillators in bulk periodically poled LiNbO₃

L. E. Myers,* R. C. Eckardt, M. M. Fejer, and R. L. Byer

E. L. Ginzton Laboratory, Stanford University, Stanford, California 94305

W. R. Bosenberg

Lightwave Electronics Corporation, Mountain View, California 94043

J. W. Pierce

Cygnus Laser Corporation, Duvall, Washington 98019

Received March 28, 1995; revised manuscript received July 12, 1995

We review progress in quasi-phase-matched optical parametric oscillators in bulk periodically poled LiNbO₃. Using the electric-field poling process, we can reliably fabricate 0.5-mm-thick crystals with uniform domain structures over a 15-mm length. Periodically poled material retains the low-loss and bulk power handling properties of single-domain LiNbO₃, and quasi phase matching permits noncritical phase matching with d_{33} , the highest-valued nonlinear coefficient. Optical parametric oscillators pumped by 1.064-μm pulsed Nd:YAG lasers have been operated over the wavelength range 1.4–4 μm with tuning by temperature or by quasi-phase-matched period. We have shown an oscillation threshold as low as 0.012 mJ with a Q-switched pump laser and pumping at greater than ten times threshold without damage. We have also demonstrated a cw doubly resonant oscillator near 1.96 μm pumped directly with a commercial cw diode laser at 978 nm. © 1995 Optical Society of America

1. INTRODUCTION

Optical parametric oscillators (OPO's) are attractive sources of coherent radiation in applications for which laser sources are unavailable or for which wide tunability is needed. Interest in OPO's has been renewed by advances in stable pump lasers and improvements in nonlinear optical materials. Still, many desirable OPO implementations are limited by problems with conventional birefringent phase-matching techniques in available materials, such as Poynting-vector walk-off, low effective nonlinear coefficient, and inconvenient phase-matching temperatures and angles.

Quasi phase matching is an alternative technique to birefringent phase matching for compensating phase velocity dispersion in frequency-conversion applications.¹ In a first-order quasi-phase-matched (QPM) device, the nonlinear coefficient is modulated with a period twice the coherence length of the interaction to offset the accumulated phase mismatch. A significant advantage of quasi-phase matching is that any interaction within the transparency range of the material can be noncritically phase matched at a specific temperature, even interactions for which birefringent phase matching is impossible. Another benefit is that the interacting waves can be chosen so that coupling occurs through the largest element of the $\chi^{(2)}$ tensor. In LiNbO₃, quasi-phase matching with all waves polarized parallel to the z axis yields a gain enhancement over the birefringently phase-matched process of $(2d_{33}/\pi d_{31})^2 \approx 20$.

Inasmuch as the pool of mature nonlinear optical

materials is limited and the development cycle for new materials is long and costly, quasi-phase matching is a useful technique for extending the range of available nonlinear optical materials. Using planar processing methods from the microelectronics industry, such as lithography, one can inexpensively fabricate practical microstructured materials for QPM interactions. The ability to pattern QPM structures allows the nonlinear material to be engineered for the desired interaction. The simplest implementation of quasi-phase matching is a single-period grating pattern that shifts the phase-matching peak to the desired operating point. Engineering more complex behavior, such as broadband phase matching or multiwavelength gratings, in principle involves only designing a more sophisticated lithographic mask.

Until recently, quasi phase matching was applied mainly to waveguide devices. Interest in the practical application of quasi phase matching to bulk nonlinear optics has been revived by the emergence of electric-field poling techniques for patterning the domain polarity of ferroelectric materials. With these techniques, periodically poled LiNbO₃ (PPLN) has been demonstrated for high-efficiency second-harmonic generation (SHG).^{2,3} We describe what are to our knowledge the first bulk QPM OPO's, made possible with the exceptional properties of PPLN now available. QPM bulk interactions greatly expand the operation range of optical parametric amplifiers and oscillators, as illustrated by the rapid succession of demonstrations and variety of configurations reported here. Our first demonstration was a pulsed singly reso-

nant QPM OPO pumped by a *Q*-switched laser. This was followed by a succession of experiments with improving material. Most recently, we demonstrated a doubly resonant QPM OPO directly pumped by a commercial cw diode laser. We expect both material and device development to continue at an accelerated rate, leading to further advances in OPO performance.

The organization of this paper is as follows. In Section 2 we introduce the theory of QPM OPO's and the implications of quasi-phase matching on tuning and bandwidth. In Section 3 we describe our methods for fabricating bulk PPLN. In Section 4 we discuss the experimental performance of our PPLN OPO's. In Section 5 we present some prospects for future research.

2. THEORY OF QUASI-PHASE-MATCHED OPO's

Much of the theory of conventionally birefringently phase-matched OPO's carries over to QPM bulk interactions with only a few simple substitutions. The substitutions are derived from a Fourier series representation of the periodically modulated nonlinear coefficient:

$$d(z) = d_{\text{eff}} \sum_{m=-\infty}^{\infty} G_m \exp(-ik_m z), \quad (1)$$

where d_{eff} is the effective nonlinear coefficient of the same process in single-domain bulk material, $k_m = 2\pi m/\Lambda$ is the grating vector of the m th Fourier component, and Λ is the period of the modulated structure. Only the Fourier component that is phase matched contributes significantly to the parametric interaction. If the nonphase-matched components are ignored, the coupled equations describing the interacting waves become⁴

$$\begin{aligned} \frac{dE_s}{dz} &= i \frac{\omega_s d_Q}{n_s c} E_p E_i^* \exp(i\Delta k_Q z), \\ \frac{dE_i}{dz} &= i \frac{\omega_i d_Q}{n_i c} E_p E_s^* \exp(i\Delta k_Q z), \\ \frac{dE_p}{dz} &= i \frac{\omega_p d_Q}{n_p c} E_s E_i \exp(-i\Delta k_Q z). \end{aligned} \quad (2)$$

From the Fourier expansion, the effective nonlinear coefficient for the QPM interaction is

$$d_Q = d_{\text{eff}} G_m. \quad (3)$$

The wave-vector mismatch for the QPM interaction is

$$\Delta k_Q = k_p - k_s - k_i - k_m, \quad (4)$$

where k_p , k_s , and k_i are the wave vectors of the pump, the signal, and the idler, respectively, assuming that all wave vectors are collinear with the grating vector. When the nonlinear coefficient is modulated with periodic sign reversal, as in PPLN, the Fourier coefficient is

$$G_m = \frac{2}{m\pi} \sin(m\pi D), \quad (5)$$

where the duty factor $D = l/\Lambda$ is given by the length l of a reversed domain divided by the period Λ of the

reversal. The effective nonlinear coefficient for quasi-phase matching is largest for a first-order process ($m = 1$) with a 50% duty factor. In this case

$$d_Q = \frac{2}{\pi} d_{\text{eff}}. \quad (6)$$

The wave-vector mismatch for the first-order QPM collinear process is

$$\Delta k_Q = k_p - k_s - k_i - \frac{2\pi}{\Lambda}, \quad (7)$$

where the period Λ is twice the coherence length l_c for the same process in single-domain material:

$$\Lambda = 2l_c = \frac{2\pi}{k_p - k_s - k_i}. \quad (8)$$

Most standard OPO theory applies to QPM OPO's. One exception occurs at high levels of conversion, where the signal wave and the idler wave act back on the pump wave, changing its phase and effectively changing the coherence length. The existing treatments for low and moderate pump conversion apply accurately to QPM OPO's, with d_Q and Δk_Q being substituted for the effective nonlinear coefficient and the wave-vector mismatch. Below we present experimental results that show good agreement with commonly used OPO threshold formulas under these conditions. Another exception is that, in approximating the spatial variation of the nonlinear coefficient with a single Fourier component, we are limiting the results to those describing the average behavior over distance. Equation (4) is the phase mismatch over many periods, not that in a single-domain region of the periodic structure. Local variation of the fields may be important for some details of OPO behavior, but this analysis is limited to a treatment of the dominant characteristics of a QPM OPO.

For discussing tuning tolerances, we use the case of a QPM parametric amplifier pumped at ω_p , with signal input at ω_s but no idler input at ω_i . In the limit of low gain, the single-pass parametric power amplification in a crystal of length L is⁴

$$G(L) = \frac{|E_s(L)|^2}{|E_s(0)|^2} - 1 \approx \frac{2\omega_s \omega_i d_Q^2 I_p}{n_s n_i n_p \epsilon_0 c^3} L^2 \operatorname{sinc}^2\left(\frac{\Delta k_Q L}{2}\right), \quad (9)$$

where I_p is the pump intensity. Phase matching is achieved when

$$\Delta k_Q = k_p - k_s - k_i - \frac{2\pi}{\Lambda} \equiv 0, \quad (10)$$

assuming a first-order collinear interaction. The first three terms of Δk_Q are the conventional phase-matching condition and hence can be adjusted by the common techniques that use angle, temperature, electric field, and pressure. The grating vector, the last term, affords an additional adjustable parameter that is especially powerful because it is independent of inherent material properties. The QPM structure is typically fabricated with a photolithographic mask and planar processing techniques, which give the designer essentially arbitrary control of the grating vector. The grating periods required

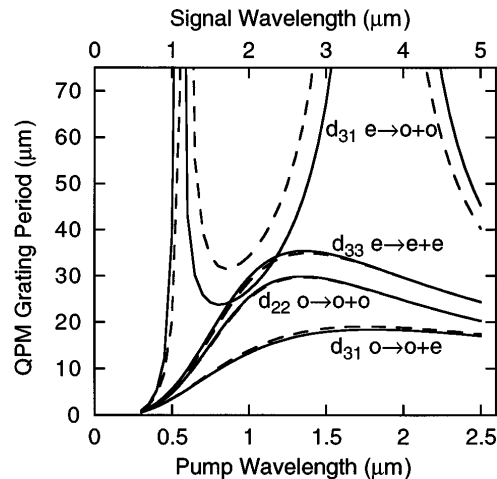


Fig. 1. First-order QPM periods of degenerate collinear OPO's in PPLN for different cases of pump \rightarrow signal + idler (e indicates an extraordinary and o an ordinary wave). The solid curves are values at 25 °C; the dashed curves are at 200 °C.

Table 1. Nonlinear Coefficients of Congruent LiNbO₃ for 1.064-μm SHG^a

$ d_{22} $	$ d_{31} $	$ d_{33} $
2.1 pm/V	4.3 pm/V	27 pm/V

^aFrom Ref. 7.

for phase matching of first-order collinear degenerate QPM OPO's are shown in Fig. 1, where Sellmeier fits are used for the dispersion of congruent LiNbO₃ and thermal expansion of the grating period is included in the calculation.^{5,6} Note that the plots in Fig. 1 can also be

used to find the grating period for QPM SHG. Of the four cases shown here, only Type-I with extraordinary-pump-producing ordinary signal and idler waves is birefringently phase matchable, which occurs at the points where the grating period becomes infinite. Interactions with orthogonally polarized beams are important in systems that employ polarization selectivity in some way. For example, a Type-II interaction is useful for a pump-resonant OPO. The interaction with all waves extraordinary is particularly interesting because of the large d_{33} nonlinear coefficient, as shown in Table 1.⁷ All the experiments reported in Section 4 used the d_{33} interaction. As a consequence of the flat dispersion of LiNbO₃ for wavelengths longer than $\sim 1 \mu\text{m}$, the required periods for infrared interactions are $>10 \mu\text{m}$, relatively large compared with those of visible interactions. This range is within the capability of our PPLN fabrication methods, as described in Section 3, which makes PPLN OPO's promising candidates for useful tunable infrared sources.

Tolerances on phase matching are determined from the full width at half-maximum of the parametric gain. From relation (9), half-maximum gain occurs at $\Delta k_Q L/2 = 0.4429\pi$. Table 2 provides a comparison of acceptance bandwidths with respect to various parameters for 1.064-μm-pumped LiNbO₃ OPO's. The results are similar to those for SHG as given by Fejer *et al.*,¹ with some differences in pump and signal wavelength acceptance because the signal and the idler are not constrained to be equal in frequency, as are the analogous fundamental waves in the SHG case. The analyses of the tolerances for pump and signal wavelength are similar for QPM and birefringently phase-matched OPO's, with the use of the proper indices in the phase-matching condition. The temperature variation of $\Delta k_Q L$ includes

Table 2. Acceptance Bandwidths for Parametric Gain of Collinear Interactions in Congruent LiNbO₃^a

Interaction ^b	Nonlinear Coefficient ^c	Angle θ (deg) ^d	Crystal Temperature (°C)	Grating Period Λ (μm)	δT^e (°C)	$\delta \lambda_p$ (nm) ^f	$\delta \lambda_s$ (nm) ^g	$\delta \nu(y-z)$ (mrad) ^h	$\delta \nu(x-z)$ (mrad) ^h
Degenerate case: $\lambda_p = 1.064 \mu\text{m}$, $\lambda_s = 2.128 \mu\text{m}$, $\lambda_i = 2.128 \mu\text{m}$									
$e \rightarrow o + o$ (B)	d_{31}	90	580	—	1.0	49	312	∞	68
$e \rightarrow o + o$ (B)	d_{eff}	45.3	25	—	4.9	12	282	71	1.2
$e \rightarrow o + o$ (Q)	d_{31}	90	25	29.0	2.8	2.0	282	102	59
$o \rightarrow o + e$ (Q)	d_{31}	90	25	14.3	7.8	0.9	5	70	70
$o \rightarrow e + o$ (Q)	d_{31}	90	25	14.3	7.8	2.8	5	70	70
$o \rightarrow o + o$ (Q)	d_{22}	90	25	27.0	38	2.8	282	97	97
$e \rightarrow e + e$ (Q)	d_{33}	90	25	31.7	19	3.2	322	105	46
Nondegenerate case: $\lambda_p = 1.064 \mu\text{m}$, $\lambda_s = 1.596 \mu\text{m}$, $\lambda_i = 3.192 \mu\text{m}$									
$e \rightarrow o + o$ (B)	d_{31}	90	566	—	1.0	3.4	10	∞	67
$e \rightarrow o + o$ (B)	d_{eff}	46.5	25	—	4.8	2.7	9.0	72	1.2
$e \rightarrow o + o$ (Q)	d_{31}	90	25	30.3	2.8	1.3	9.0	104	59
$o \rightarrow o + e$ (Q)	d_{31}	90	25	17.1	13	1.1	3.7	77	77
$o \rightarrow e + o$ (Q)	d_{31}	90	25	11.9	5.4	12	2.1	64	64
$o \rightarrow o + o$ (Q)	d_{22}	90	25	25.9	42	12	9.0	95	95
$e \rightarrow e + e$ (Q)	d_{33}	90	25	30.6	22	10	11	103	46

^aAll the values are calculated for a single pass in a 1-cm-long crystal, with Sellmeier coefficients from Ref. 5.

^bPump \rightarrow signal + idler. (B) Refers to birefringently phase-matched interactions; (Q) indicates quasi phase matching.

^cSee Table 1 for values. For critical phase matching, $d_{\text{eff}} = |d_{31}|\sin \theta + |d_{22}|\cos \theta \approx 4.5 \text{ pm/V}$.

^dAngle of the crystal optic axis relative to the propagation direction.

^eTemperature acceptance FWHM. Thermal expansion coefficients are from Ref. 6.

^fPump wavelength acceptance FWHM for fixed λ_s .

^gSignal wavelength acceptance FWHM for fixed λ_p .

^hAngle acceptance FWHM for fixed λ_p , λ_s , and λ_i . The crystal optic axis is in the $x-z$ plane; domain boundaries are parallel to the $y-z$ plane. Phase-matched propagation is in the x direction, and ν is the angular deviation of the pump from phase matching. The signal and the idler change direction but remain collinear as ν is varied. See Fig. 2 of Ref. 1.

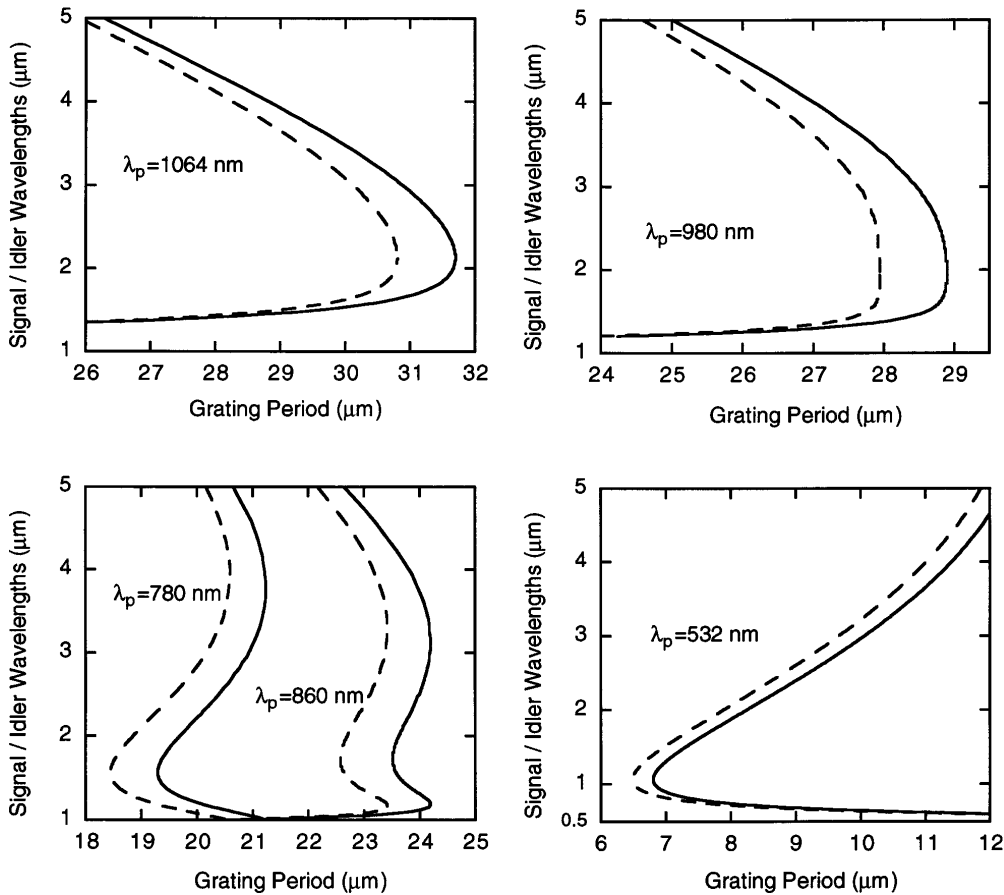


Fig. 2. First-order QPM periods for collinear PPLN OPO's with common pump lasers. All the waves are polarized parallel to the crystal z axis. The solid curves are at 25°C ; the dashed curves are at 200°C .

the thermal expansion of the grating period $\Lambda(T)$ in addition to the thermal expansion of the crystal length $L(T)$ and the temperature variation of the refractive indices. For LiNbO₃ the temperature dependence of the dispersion is generally less than that of the birefringence, so the temperature acceptance can be quite large for interactions with parallel-polarized waves. In these cases the thermal expansion of the grating period can be a significant factor in the phase-matching condition. Compared with SHG, angular dependence of phase matching has the additional complication that the signal and idler waves can have independent propagation directions. When the pump wave is propagating at some angle relative to the grating vector, then at least one of the other two waves must be noncollinear with both the pump and the grating to maintain the boundary-condition requirements on the phase mismatch. The difference in the propagation directions of the interacting waves results in an effective interaction length for the gain similar to that observed in birefringently phase-matched OPO's with noncollinear phase matching or Poynting-vector walk-off. In an actual OPO the relationship between the signal and the idler directions will be a compromise among the phase-matching, the walk-off, and the resonator constraints. For the angular tolerances presented here the signal and idler are collinear, comparable with those in the SHG analysis considered by Fejer *et al.*¹ A significant result of that analysis is that the interaction is noncritical whenever propagation is collinear with the grating vector.

This is seen in Table 2, which shows that the QPM interactions have angular acceptance comparable with those in the noncritical birefringently phase-matched case.

In Fig. 2 we show tuning curves, i.e., the locus of points where $\Delta k_Q = 0$, of collinear OPO interactions in PPLN pumped by common lasers. For 1.064- μm Nd:YAG lasers, and Ti:sapphire and diode lasers from 780 to 980 nm, the grating periods are comfortably attained in PPLN. For a green-pumped OPO, the grating periods as small as 6.8 μm are on the short end of our current bulk processing methods but are achievable. Note that the tuning curves of the 780–860-nm-pumped OPO's turn back on themselves because these interactions straddle the region in which the curvature of the dispersion changes sign. A consequence of this behavior is that the parametric gain bandwidth is extremely large, which implies the interesting prospect of a high-bandwidth parametric amplifier in the optical communication band.⁸

A grating period can be selected to permit noncritical phase matching of the desired interaction at a given temperature. This was the design approach taken in the experimental demonstrations presented in Section 4 below. However, QPM design is not limited to gratings with a single period; more sophisticated structures give specialized phase-matching behavior. For example, multiple grating periods could be superimposed so that the device simultaneously produces frequency conversion to multiple wavelengths. Fourier synthesis is a strategy for designing more complicated QPM structures.¹ By planar

microprocessing techniques, in principle any pattern that can be represented with a lithographic mask can be fabricated in the material. Broadening the phase-matching acceptance bandwidth is one example to which this advanced engineering control has been applied.⁹ A widely tunable OPO with a fanned grating design is described in Section 5.

In summary, standard OPO analysis can be applied to QPM OPO's with a straightforward redefinition of the nonlinear coefficient and wave-vector mismatch. The grating vector affords a powerful additional tool in tailoring phase matching and permits OPO design options that are now available only with the practical implementation of QPM devices. Any collinear interaction within the transparency range of the material can be noncritically QPM at a given temperature, even those for which birefringent phase matching is not possible. In LiNbO₃, interaction with all waves polarized parallel to the crystal optic axis has a nonlinear drive that is a factor of 20 higher than the largest available in birefringently phase-matched processes. Quasi phase matching permits engineering the phase-matching behavior rather than relying on inherent material properties, so, in some sense, quasi phase matching replaces the search for new nonlinear optical materials with the search for patterning techniques of existing materials. Widely tunable infrared OPO's are possible with our current PPLN fabrication methods, described in Section 3.

3. FABRICATION OF PPLN

Implementation of quasi-phase matching requires a fabrication method that can achieve uniform micrometer-scale periodic structures while preserving the material's transparency, nonlinearity, and power handling capability. Quasi phase matching was initially proposed before birefringent phase matching,¹⁰ but difficulties in fabricating QPM materials have presented its widespread use in bulk devices. Recent advances in fabricating practical QPM materials have renewed interest in this approach. LiNbO₃ has attracted special attention because it is a mature, readily available material with transparency covering a useful range from 0.35 to >4 μm . Quasi phase matching can be implemented in a ferroelectric material such as LiNbO₃ by periodic reversal of the ferroelectric domains because antiparallel domains correspond to a sign reversal of the nonlinear coefficient. Several techniques have been developed for producing PPLN. Chemical indiffusion has been used to make periodic structures of good quality; however, the pattern is limited to shallow layers, which are sufficient for wave-guide devices but not deep enough for bulk devices.^{11,12} Bulk PPLN has been made by modulation of the crystal growth process, but it suffers from axial variations in domain periodicity that significantly degrade efficiency.^{13,14} Electron-beam writing can produce bulk PPLN with good periodicity, but reproducibility is poor, and the process does not lend itself to commercial manufacturing.¹⁵ Recently techniques for ferroelectric domain reversal with an external electric field have produced PPLN^{2,3,16} and periodically poled LiTaO₃ (Ref. 17) and KTiOPO₄ (KTP) (Ref. 18) for QPM SHG. In this approach, domain periodicity is precisely defined by a lithographic mask by

standard microfabrication techniques. We recently developed an electric-field poling process that yields uniform PPLN in thick substrates for efficient QPM frequency-conversion applications.^{19,20}

We use standard optical-grade LiNbO₃ wafers of congruent composition with the arrangements shown in Fig. 3. The positive electrode with the desired structure is patterned on the +z surface of the wafer. We have used two variants for this electrode fabrication. In the first approach, a 0.2- μm -thick Al grating is patterned by lift-off lithography. A 2- μm -thick layer of photoresist is applied over the grating, leaving a portion of the metal pattern exposed. Contact is made to the exposed metal with a liquid electrolyte consisting of LiCl in deionized water. In the second variant, a grating pattern of photoresist is covered by an Al film and then covered by the electrolyte. In both cases the photoresist layer insulates the electrode lines, inhibits domain growth between the grating lines, and forms the contour of an isopotential surface when covered with the electrolyte. The isopotential surface controls fringing fields at the edges of the grating lines, improving pattern uniformity and resolution. The first method (insulator over conductor) produces better pattern fidelity, possibly because the well-defined edges of the metal lines provide a more homogeneous field condition than the tapered photoresist edges in the second method. The second method (conductor over insulator) is easier to fabricate with a single lithography step, and it provides pattern quality sufficient for devices with large feature size. We also patterned the +z surface directly with photoresist trenches and liquid contact,¹⁶ but we found that the metal–LiNbO₃ contact can enhance the poling. For the negative electrode, liquid electrolyte is applied directly in the bare -z surface. The liquid electrode fixture consists of two electrolyte-containing chambers, which squeeze the LiNbO₃ sample between O rings. This arrangement permits application of fields exceeding 25 kV/mm without breakdown of the sample and without the need for surrounding oil or vacuum. The choices of Al for the metal, photoresist for the insulator, and LiCl solution for the liquid contact are convenient but not necessarily optimal, making this an area for future research efforts.

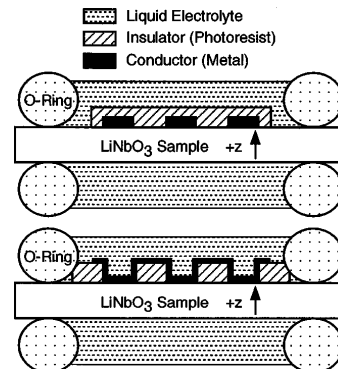


Fig. 3. Electrode configurations for electric-field poling. The upper figure shows a variant with insulator over conductor; the lower figure shows conductor over insulator. In both cases the covering electrolyte connects the sample to the circuit and forms an isopotential surface that helps to control fringing fields around the pattern.

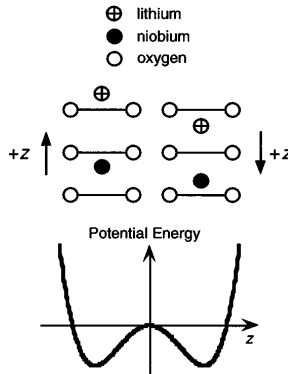


Fig. 4. Qualitative picture of ferroelectricity in LiNbO_3 . Polarity of the two stable-domain orientations is determined by the direction of offset of the metal ions relative to the oxygen layer. Domain polarity can be reversed by application of a field sufficient to move the ions from the one stable location to the other.

A qualitative picture of ferroelectricity in LiNbO_3 is shown in Fig. 4. Polarity of a ferroelectric domain is determined by the offset of the metal ions either above or below the oxygen layers.²¹ Domain reversal involves reorienting the crystal from one stable configuration to the other, which can be effected by the application of an external electric field. Significant domain reversal occurs when the applied field exceeds a certain value referred to as the coercive field, which is $\sim 21 \text{ kV/mm}$ for LiNbO_3 at room temperature. Domain reversal is permanent after roughly 50 ms. When the voltage is abruptly turned off, domains that switched polarity in the last $\sim 50 \text{ ms}$ will return to their original polarity. For slow poling, such as we typically use, this backreversal is negligible. However, when the poling rate is fast, the material that reverts to its original polarity may represent a sizable portion of the domain-reversed region. Continuing to apply voltage for $\sim 50 \text{ ms}$ after poling, for instance, at a level that is half the coercive field value, ramping the voltage off gradually on the time scale of 50 ms, and blocking backflow of charge with a series diode are effective means of preventing backreversal of domains. Poling with shorter pulses (e.g., $\sim 100 \mu\text{s}$) can also be done with a voltage source with a circuit topology that connects it to the sample through a switching element. In this case, turning off the voltage pulse places the switch in a high impedance state that blocks the backflow of charge from the sample, allowing the domain reversal to become permanent. After domain reversal has been accomplished and the field removed, we have seen that the new domain orientation is stable even at temperatures exceeding 800°C .

The poling circuit consists of a high-voltage source with a series resistor R_s , as shown in Fig. 5. Typical oscilloscope traces of voltage and current measured during poling are shown in Fig. 6. With no sample in the circuit, the high-voltage supply V_1 is set to produce a voltage pulse at V_2 that exceeds the coercive voltage. When the same voltage pulse is applied to the sample, current flows through the circuit as the domain polarity reverses. The voltage drop in the series resistor lowers the voltage on the sample, leading to a decrease in the poling rate. Decreasing poling current raises the voltage on the sample. These competing effects cause the voltage on the sample

to clamp at the coercive field level. Current flow in the circuit is regulated by the values of the series resistor R_s and the driving voltage V_1 .

The poling current I_{pol} is given by

$$I_{\text{pol}} = \frac{V_1 - V_c}{R_s} - \frac{V_c}{R_{\text{vm}}}, \quad (11)$$

where V_1 is the supply voltage before the series resistor R_s , V_c is the voltage corresponding to the coercive field level ($\sim 21 \text{ kV/mm}$), and R_{vm} is the impedance of the voltage monitor. Current of $13\text{--}33 \mu\text{A}$ was used to pole the devices reported in this paper. By varying the driving voltage V_1 and the series resistance R_s , we performed testing at currents of as much as 10 mA, but the lower current tended to produce straighter domain walls. With constant current, the duration of poling depends linearly on the area being poled. The charge Q transferred to the sample is that required for compensation of the reversed orientation of the spontaneous polarization, given by $Q = 2P_s A$, where P_s is the spontaneous polarization of LiNbO_3 , A is the area of the domain-reversed region, and the factor of 2 accounts for the polarity reversal. A published value²² of P_s is $71 \mu\text{C}/\text{cm}^2$, but we found that a value 10% higher gives better agreement in our research.

We accomplish patterning by controlling the charge transfer that accompanies domain reversal. Domain growth is almost instantaneous in the z direction, so the poling current represents primarily lateral domain growth in the x and y directions. The conductivity of LiNbO_3 at room temperature is low enough that the poling current can be monitored readily. The oscilloscope

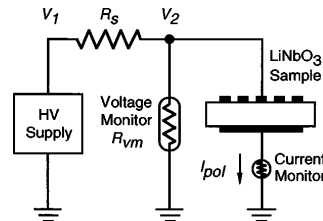


Fig. 5. Electric-field poling circuit. Typically $R_s = 100 \text{ M}\Omega$, $R_{\text{vm}} = 1 \text{ G}\Omega$, and V_2 is set at 12 kV with no sample in the circuit. During poling, V_2 clamps at the coercive voltage $V_c \approx 10.5 \text{ kV}$ for a 0.5-mm-thick LiNbO_3 sample.

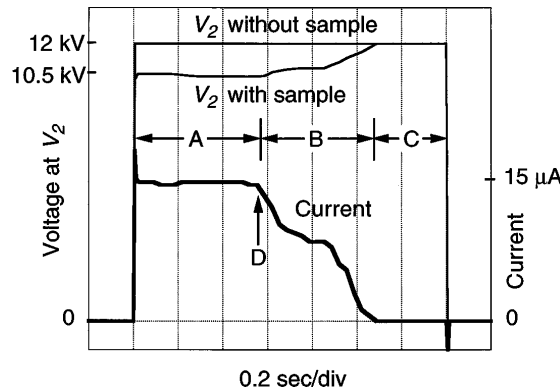


Fig. 6. Voltage and current waveforms for poling a 3-mm-diameter, 0.5-mm-thick piece of LiNbO_3 . Section A, poling under the metal or liquid contact. Section B, poling under the photoresist. Section C, after completion of poling. For a patterned device, the voltage would be turned off at point D.

trace in Fig. 6 shows the poling current and voltage for a 3-mm-diameter sample with a patterned electrode on the $+z$ surface. The initial plateaus (section A) in the current and voltage indicate poling taking place under either liquid or metal in direct contact with the LiNbO_3 . The middle region (section B) with lower current indicates poling under the photoresist at a higher coercive voltage. The end of the pulse (section C) where no current flows indicates completion of domain reversal. The strategy for domain patterning is to stop the voltage pulse before the poling progresses under the photoresist (point D). We typically do this by limiting the pulse duration at a given current and driving voltage level while monitoring the current and charge transfer. Another approach is to pole with an applied field just slightly above the coercive field of the conductor-covered material but low enough to prevent poling under the insulator-covered region. The series impedance can be adjusted or eliminated to achieve the desired poling rate. Computer control is useful in monitoring poling and determining a stopping criterion.¹⁷

The domains typically grow beyond the width of the metal electrode defined by the grating lithography as the result of the remaining fringing fields along the edges. For devices with periods of interest for infrared applications (i.e., periods $> 10 \mu\text{m}$), a rule of thumb is that the domain width will be $\sim 3\text{--}4 \mu\text{m}$ wider than the electrode width. The electrode structures described above are effective in making this domain width uniform over the poled region. The lithography pattern can be adjusted to take into account the resultant domain size. Shown in Fig. 7 is a cross-sectional view of a PPLN sample, illustrating the straight, vertical domain boundary walls throughout the material volume. We currently fabricate 0.5-mm-thick device-quality PPLN with 15-mm-long poled regions. We expect to be able to make PPLN 1 mm thick and 5 cm long in future research.

To verify domain pattern homogeneity for infrared parametric interactions, we performed a difference-frequency generation experiment, using a sample with a $15.5\text{-}\mu\text{m}$ grating period similar to that shown in Fig. 7. The end faces of the crystal were cut and polished at the periodically poled region such that the finished device was 2.2 mm long. Pump radiation from a cw Ti:sapphire laser tunable near 710 nm and signal radiation from a $1.555\text{-}\mu\text{m}$ cw erbium fiber laser were mixed in the PPLN crystal. The single-pass idler power generated near $1.3 \mu\text{m}$ is shown in Fig. 8, along with the theoretical tuning curve. The ripples in the measured data are due to Fresnel reflection interference from the uncoated polished end faces of the crystal. The theoretical curve is calculated from the Sellmeier coefficients for bulk LiNbO_3 at room temperature; the phase-matching peak has been shifted +1 nm by a change in the dispersion of $\sim 10^{-4}$, which is within the accuracy claimed for the Sellmeier fit. The significance of this result is that the tuning curve shows a single well-defined peak with near-theoretical bandwidth, demonstrating coherent interaction over the length of the sample.

Over most of its transparency range, the intrinsic material loss of LiNbO_3 is negligible. For example, a LiNbO_3 monolithic total-internal-reflection (TIR) resonator was recently demonstrated with a finesse of 6000, corresponding to a loss of less than 0.1% from the 16-mm path

length and three TIR bounces.²³ However, with periodically poled material there is concern that scattering or absorption at the domain wall interfaces could contribute noticeable loss. Because of the large number of domain walls encountered in any appreciable interaction length, even a small amount of loss added at each domain wall would limit the utility of the material for some OPO applications. Qualitatively, we observed no difference in visible scatter when transmitting a He–Ne beam through regions of the same crystal with and without periodic pol-

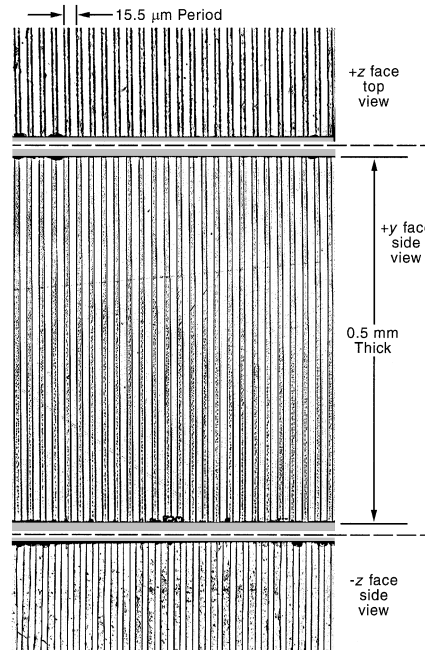


Fig. 7. Orthographic view of 0.5-mm-thick PPLN with a $15.5\text{-}\mu\text{m}$ period, after etching in HF acid to reveal the domain structure. The three panels are top, side, and bottom views taken at the same location in the crystal by cutting and polishing into the grating region. The top panel is the $+z$ face upon which the lithographic electrode was applied. The middle panel is a cross-sectional view of the $+y$ face. The bottom panel is the $-z$ face, which had the unpatterned ground electrode.

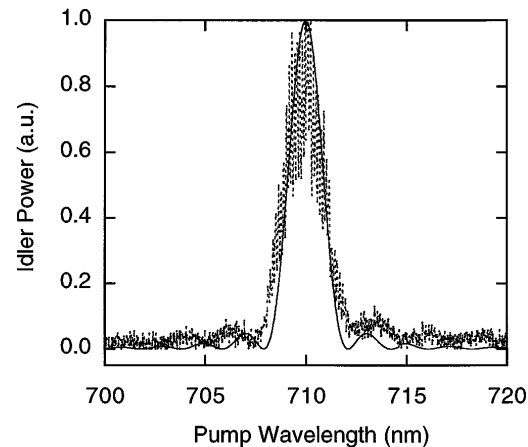


Fig. 8. Difference-frequency generation tuning curve for $15.5\text{-}\mu\text{m}$ period, 2.2-mm-long PPLN, with $\lambda_s = 1.555 \mu\text{m}$ and $\lambda_i \approx 1.3 \mu\text{m}$. The calculated curve (solid curve) is based on the Sellmeier coefficients at 25°C with the peak shifted +1 nm to match the data. The fringes in the data are due to Fresnel reflections from the uncoated end faces.

ing. We quantitatively measured loss by placing PPLN crystals in an optical resonator with a bare-cavity finesse of 200, pumped by a single-frequency cw Tm:YAG laser at $2.014\text{ }\mu\text{m}$. We tested PPLN pieces with 31- and $28.5\text{-}\mu\text{m}$ periods that were antireflection (AR) coated with a multilayer coating centered at $1.84\text{ }\mu\text{m}$. Spectrophotometer measurements of the coating on witness samples gave power loss at $2.014\text{ }\mu\text{m}$ of $0.3\%/\text{surface} \pm 0.05\%$. By measuring the finesse of the resonator with and without the PPLN crystal for several samples 9 and 15 mm long, we found that the range of single-pass power loss was $0.4\%-0.8\% \pm 0.2\%$, uncorrelated with sample length. This loss value is the integrated total, which includes losses both from coated surfaces and from propagation through the crystal. Within our resolution limits there appears to be no measurable loss from the material itself compared with that of the coatings. Because the number of domain walls ranged from 600 to 1000 in these pieces, we conclude that periodic poling adds no loss to that of single-domain LiNbO₃. Low loss is of critical importance in many OPO applications.

4. PPLN OPO EXPERIMENTS

The success in fabricating PPLN material led to a rapid succession of QPM OPO demonstrations. Our first device-quality pieces were 5 mm long. With these short lengths we took advantage of the high gain from *Q*-switched laser pulses to demonstrate our first QPM OPO in a bulk nonlinear optical material. In the months following the initial demonstration our processing methods developed, and we produced PPLN crystals more than 15 mm long, which allowed us to perform a variety of OPO experiments. Long lengths of this material with low loss and high nonlinear drive permitted low-threshold devices, including long pulse and cw operation. All the PPLN OPO's described here used collinear interactions with $d_Q = (2/\pi)d_{33}$.

A. PPLN OPO's Pumped by *Q*-Switched Nd:YAG Lasers
The typical setup for our *Q*-switched laser-pumped experiments is shown in Fig. 9. The OPO resonator is a linear cavity with mirrors selected to resonate at the signal as a singly resonant oscillator (SRO). We demonstrated our first bulk QPM OPO by using a 5-mm-long PPLN crystal having a 31- μm period.¹⁹ The pump laser was an acousto-optically *Q*-switched, quasi-cw diode-pumped Nd:YAG laser operating at $1.064\text{ }\mu\text{m}$ with a beam-quality measure $M^2 = 1.8$. The laser produced pulses with 7-ns full width at half-maximum at 100 Hz. The input cavity mirror had a 6.7-cm radius of curvature with $R_p = 6\%$, $R_s = 99\%$, and $R_i = 40\%$, where R_p , R_s , and R_i are the mirror reflectivities at the pump, the signal, and the idler wavelengths, respectively. The output coupler was flat, with $R_p = 56\%$, $R_s \approx 70\%$, and $R_i \approx 20\%$. The mirror separation was 22 mm, giving a waist of $100\text{ }\mu\text{m}$ for an optimally mode-matched pump; the actual pump beam was $177\text{ }\mu\text{m}$ in the crystal. The PPLN end faces were AR coated near $1.8\text{ }\mu\text{m}$ with a single layer of SiO₂, with pump transmission of $T_p \approx 86\%$. As shown in Fig. 10, this SRO produced output continuously tunable from 1.66 to $2.95\text{ }\mu\text{m}$, with the crystal temperature varying from room temperature to $180\text{ }^\circ\text{C}$.

The measured tuning curve matches the design prediction within the accuracy of the Sellmeier fit. Using a different piece of PPLN with a $28.5\text{-}\mu\text{m}$ period, we measured signal and idler wavelengths at 1.45 and $4.0\text{ }\mu\text{m}$, respectively, at room temperature. The linewidth of the signal beam is shown in Fig. 11. The theoretical curve is based on the single-pass gain from relation (9) narrowed by a factor of approximately the square root of the number of passes of the signal pulse in the cavity as described by Brosnan and Byer.²⁴

The measured threshold was near the theoretical value predicted by a simple model of a pulsed SRO with loosely focused Gaussian beams²⁴:

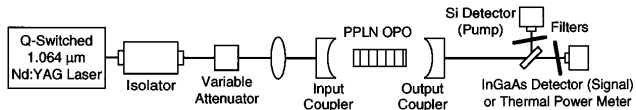


Fig. 9. Setup for OPO experiments with a *Q*-switched $1.064\text{-}\mu\text{m}$ Nd:YAG pump laser.

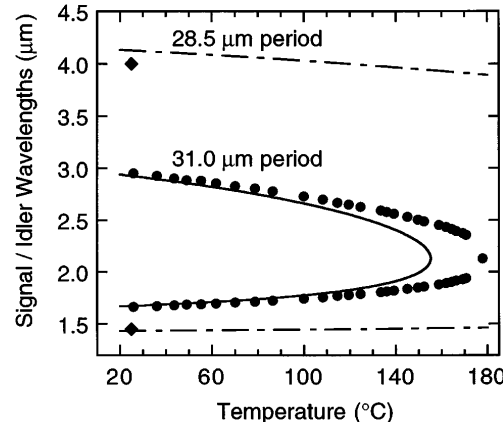


Fig. 10. Temperature tuning curves for $1.064\text{-}\mu\text{m}$ -pumped OPO in bulk PPLN with 31- and $28.5\text{-}\mu\text{m}$ periods. The calculated curves are based on the Sellmeier coefficients and include thermal expansion. The offset between the data and theory is within the accuracy of the Sellmeier fit.

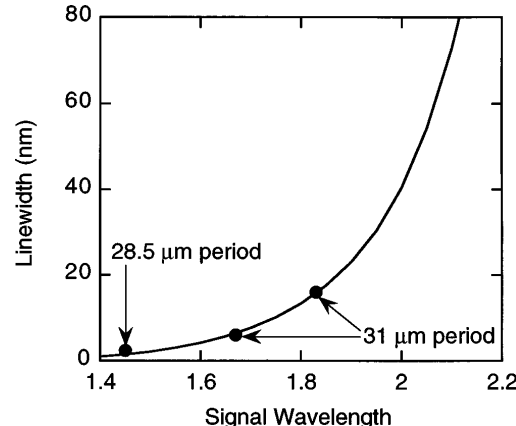


Fig. 11. Linewidth of PPLN OPO pumped by a $1.064\text{-}\mu\text{m}$ *Q*-switched Nd:YAG laser. The theoretical curve is the single-pass gain narrowed by a factor of approximately the square root of the number of passes of the signal pulse in the cavity.

$$J_T = \frac{1}{T_p} \frac{n_p n_s n_i \epsilon_0 c^3}{2\omega_s \omega_i d_Q^2} \frac{2.25}{L^2} \frac{w_p^2 + w_s^2}{w_p^2} \frac{\tau}{(1 + \gamma)^2} \times \cosh^{-1} \left(\frac{30L_{\text{cav}}}{2\tau c} + a_d - \ln \sqrt{R_s} \right), \quad (12)$$

where J_T is the threshold pump fluence; T_p is the pump transmission through the input coupler and the crystal surface; L is the crystal length; w_p and w_s are the Gaussian mode field radii of the pump and the signal, respectively; τ is the $1/e^2$ half-width of the pump-pulse duration; γ is the ratio of backward to forward pump-field amplitudes in the crystal ($\gamma = 0.6$ in this calculation); L_{cav} is the cavity optical length; $a_d = 0$ is the single-pass power loss at the signal, not including the output coupling; and R_s is the signal reflectivity of the output coupler. The nonlinear coefficient is $d_Q = 14.4 \text{ pm/V}$, where d_{eff} has been adjusted for constant Miller delta.²⁵ The calculation gives 0.191 mJ, which is near our measured value of 0.135 mJ at 145 °C, where $\lambda_s = 1.83 \mu\text{m}$. By increasing the pump energy to damage the crystal intentionally, we obtained damage at 1.4 mJ, which agrees with previous reports for damage fluence of single-domain LiNbO₃ of 3 J/cm² in a 10-ns pulse.²⁴ The factor-of-10 margin between oscillation threshold and damage limit indicates the potential utility of PPLN OPO's of this type. The key results of this experiment were that no excess loss in the PPLN material was observed and that the damage limit was unchanged from its value for single-domain LiNbO₃.

A side-by-side comparison with a KTP OPO illustrates the high gain available from PPLN. We used a 20-mm-long KTP crystal, x cut for Type-II noncritical [$d_{32} = 3.6 \text{ pm/V}$ (Ref. 7)] phase matching at room temperature with $\lambda_s = 1.57 \mu\text{m}$ and AR coated for the pump and the signal wavelengths. The PPLN crystal was 5.2 mm long with a 31-μm QPM period for $\lambda_s = 1.66 \mu\text{m}$ at room temperature, similar to the piece described in the preceding paragraph. The experimental layout was similar to that of Fig. 9, but with a different pump laser and cavity mirrors. The pump laser was an acousto-optically Q-switched cw diode-pumped Nd:YAG laser operating at 1.064 μm, with a 7-ns pulse length, a repetition rate of 1 kHz, and $M^2 = 1.2$. The cavity input and output couplers had 57-mm radii of curvature with $R_p = 7\%$, $R_i < 10\%$, and $R_s = 99\%$ for both the PPLN and KTP signal wavelengths. The pump beam was focused to a 90-μm waist in the crystals. The mirror separation was adjusted to give the same optical cavity length of 35 mm for both crystals to equalize the number of cavity round trips during the pump pulse. The measured thresholds were 0.110 mJ for the KTP and 0.145 mJ for the shorter PPLN crystal. The ratio of the measured thresholds agrees with that of the gains calculated from relation (9), assuming no loss and ideal quasi-phase matching.

With the longer PPLN crystals that became available as our processing developed we investigated low-threshold operation in a configuration with closer to optimized focusing. We used a 15-mm-long PPLN piece with a 31-μm period. The end faces of the crystal were AR coated for room-temperature operation with $\lambda_s = 1.66 \mu\text{m}$ ($R_p = 5\%/\text{surface}$, $R_s = 0.8\%/\text{surface}$). The pump laser was the same as described in the preceding paragraph, focused in the crystal to a spot size

of $w_p = 47 \mu\text{m}$, which gives a ratio of crystal length L to confocal parameter $b = 2\pi n_p w_p^2 / \lambda_p$ of $L/b = 0.53$. The cavity mirrors both had 25-mm radii of curvature with a separation of 33 mm, so the waist of an optimally mode-matched pump beam would be 65 μm. The input coupler had reflectivities of $R_p = 14\%$, $R_s = 98\%$, and $R_i = 10\%$; the output coupler had reflectivities of $R_p = 5\%$, $R_s = 92\%$, and $R_i = 30\%$. The threshold of this PPLN OPO was 0.012 mJ. The low threshold available with PPLN makes it an excellent choice for OPO's pumped by cw diode-pumped Q-switched solid-state lasers.

With the performance demonstrated in the experiments at 100 Hz–1 kHz described above, a straightforward way to increase the average power is to increase the pulse-repetition rate. The repetition rate of our laser was adjustable from 0 to 40 kHz; the pulse length was 7 ns at 1 kHz and 19 ns at 10 kHz. The pulse energy of the pump laser drops off with increasing repetition rate; however, the low threshold of a PPLN OPO means that high-repetition-rate operation can still be achieved. Initially, our attempts at high-repetition-rate operation were hindered by photorefractive damage owing to extraneous visible-light generation. For example, with a 31-μm-period piece at room temperature ($\lambda_s = 1.66 \mu\text{m}$), we observed red at ~0.650 μm, green at 0.532 μm, and blue at ~0.467 μm. The red is the sum frequency of the signal and the pump, and the blue appears to be the sum frequency of the doubled signal and the pump. The green is the second harmonic of the pump, which is not phase matched but is enhanced compared with green generated in a single coherence length. Typically the green and the red outputs have comparable powers, whereas the blue is more than an order of magnitude lower. Of these, the green light is the largest contributor to photorefractive damage. PPLN has been shown to be less susceptible to photorefractive damage than single-domain LiNbO₃ in visible-light SHG experiments, probably because of a cancellation effect in the alternating domains.^{13,16,26} However, in the infrared the domain lengths are nearly 10 times longer, which gives less average cancellation, and even a small loss owing to remaining photorefractive damage can have a significant effect on the OPO threshold.

We measured photorefractive damage in an OPO by using a 28.5-μm-period, 9-mm-long PPLN crystal that was AR coated for the signal wavelength. The input and the output couplers had 37.3-mm radii of curvature, were separated by 42 mm, and had signal reflectivities of >99% and 90%, respectively. The pump laser was the same as that described above, focused to a 47-μm waist in the crystal. We varied the pump power by changing the repetition rate while keeping the pulse energy fixed at 0.100 mJ. For pumping at 0.1 W_{av} (3 kW_{av}/cm² at the focus), which produced 0.3 mW_{av} (17 W_{av}/cm²) of green light, the OPO was unaffected by photorefractive damage. For pumping at 0.5 W_{av}, the OPO output decayed from its initial value on the scale of a few minutes, reaching a steady state at half its initial value. At 1 W_{av} the OPO quickly decayed and ceased to operate in 1 min. Degradation of the OPO output was accompanied by evident fanning in the green beam, which is a typical indicator of photorefractive damage.²⁷ Photorefractive damage is not permanent; one can erase it by heating the crystal so that the carriers causing the refractive-index

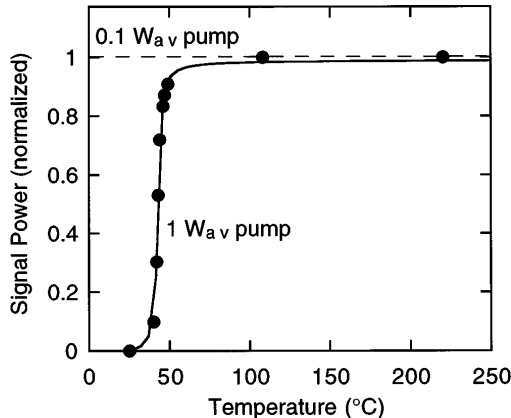


Fig. 12. OPO output for a 1-W_{av} pump (100 μ J, 10 kHz) at 1.064 μ m, showing real-time erasure of photorefractive damage with increasing temperature. For a 0.1-W_{av} pump, the same OPO operated without degradation at room temperature.

perturbation are diffused. It is also well known that one can erase photorefractive damage in real time by simultaneously heating the crystal and exposing it to the damaging light,²⁷ and we applied this principle in our high-repetition-rate OPO experiments. (Other ways of eliminating photorefractive damage are discussed in Section 5.) In Fig. 12 the steady-state value of the OPO pumped with 100 μ J at 10 kHz is plotted versus the crystal temperature. The 28.5- μ m-period PPLN has negligible tuning over the temperature range considered here, as shown in Fig. 10, so gain parameters were constant as we changed the temperature of the crystal. Near 50 °C there is a steep improvement in the performance, indicating that loss induced by photorefractive damage is eliminated. Pumping with 1 W_{av} (100 μ J at 10 kHz), we measured 220 mW_{av} at $\lambda_s \approx 1.45 \mu$ m and 34 mW_{av} at $\lambda_i \approx 4 \mu$ m. The importance of this experiment is that photorefractive damage can be controlled with operation at temperatures in the 60–100 °C range, allowing the average power of the pump source to be increased while maintaining noncritical phase matching with quasi-phase matching.

The high gain of PPLN is made possible through the large d_{33} component of the nonlinear susceptibility tensor. Another feature of having all the waves polarized in the same direction is that the use of Brewster surfaces is a convenient design option. We fabricated Brewster surfaces on the end faces of a 15-mm-long PPLN crystal having a 31- μ m period. We used this piece in an OPO with the same pump laser described in the preceding paragraph. The input coupler had a 25-mm radius of curvature with $R_p = 7\%$, $R_i < 10\%$, and $R_s = 99\%$; the output coupler was a flat mirror with $R_s = 93\%$. The pump was operated at 1 kHz and was focused at a 47- μ m spot as in the preceding paragraphs. Incidence at Brewster's angle ($\theta_B = 65^\circ$ for 1.064 μ m) results in a spot size on the crystal surface larger by a factor of $1/\cos \theta_B = 2.4$ and a pump waist in the crystal larger by a factor of $\tan \theta_B = n_p = 2.2$. We measured a threshold of 0.026 mJ. Pumping at eight times threshold (0.200 mJ/pulse), we measured 71% pump depletion, as shown in Fig. 13. Inasmuch as the PPLN itself has low losses, with optimized mirrors most of the converted power should be extractable. The Brewster-angle surface can help to obviate the need for

broadband, damage-resistant coatings. The low losses available with Brewster surfaces and the surface intensity reduction that is due to the nonnormal geometry have the potential of extending the envelope of low-threshold, high-throughput OPO's.

In summary, our experiments with Q-switched Nd:YAG pump lasers show that PPLN is an exceptional material for OPO applications. Our success in fabricating device-quality PPLN permitted the demonstration of a bulk QPM OPO. Further processing developments provided better material, leading to a number of QPM OPO devices. The envelope of performance of these experiments covered operation with low threshold (0.012 mJ), high pump conversion (70%), pumping without damage at ~ 10 times above threshold, and pumping with over 1-W average power.

B. Long-Pulse PPLN OPO

Taking advantage of the high-gain and low-optical-loss properties of PPLN demonstrated in our experiments with Q-switched lasers, we have operated a low-peak-power (<100 W) long-pulse OPO.²⁸ OPO's are usually grouped by their temporal characteristics, and recently most attention has been given to 10–30-ns pulse, 100-fs–1-ps pulse, and cw OPO's.²⁹ The device described in this section is an OPO that operates in the 0.1–1-ms pulse range, a regime that has received virtually no attention but that offers the potential of producing narrow-linewidth output without the complexities associated with shorter-pulse OPO's.

The pump source architecture used here is the master-oscillator–power-amplifier configuration shown in Fig. 14. The master laser consists of a cw, diode-pumped, Nd:YAG single-frequency laser (700-mW output

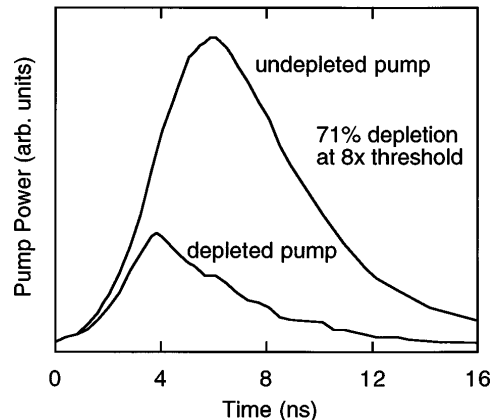


Fig. 13. Pump pulse transmitted through the OPO cavity with the OPO off (upper trace) and the OPO on (lower trace). The difference between the traces indicates the pump depletion.

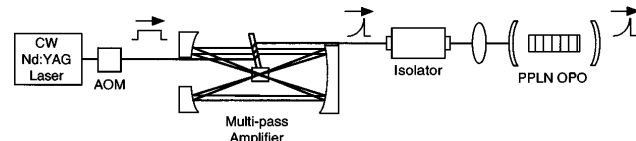


Fig. 14. Experimental setup for a long-pulse PPLN OPO. The 700-mW 1.064- μ m cw laser is chopped with an acousto-optic modulator (AOM) to produce rectangular pulses, which are amplified to ~ 300 -W peak power with the pulse shape shown in Fig. 15. Pulse duration, pulse shape, and repetition rate can readily be varied with the acousto-optic modulator.

at 1.064 μm), which is acousto-optically modulated before being sent through a 16-pass Nd:YAG amplifier.³⁰ The temporal laser pulse shape can, in principle, be electronically controlled by application of the proper rf waveform to the acousto-optic modulator. In our experiment we used the rf to shutter the master laser to produce a rectangular pulse, with peak power ~ 600 mW and duration varying between 150 ns and cw. The amplifier alters the rectangular pulse that is due to gain saturation to the shape shown in Fig. 15. The square pulse input was chosen to produce the highest peak power in the amplified pulse. The amplified pump beam has peak power of ~ 300 W with a beam-quality measure of $M^2 = 1.2$.

The PPLN crystal for this experiment was 15 mm long with a 31- μm QPM period for signal and idler wavelengths of 1.67 and 2.93 μm , respectively, at room temperature. The flat end faces were AR coated, giving $R_p = 5\%/\text{surface}$ and $R_s = 0.8\%/\text{surface}$ (the coating was designed for minimum reflection at 1.96 μm). The OPO resonator was a linear cavity with two identical mirrors having 15-mm radii of curvature and reflectivities of $R_p = 14\%$, $R_s = 98\%$, and $R_i = 12\%$. The round-trip feedback of the idler was $<1.4\%$, which made the OPO behave as a singly resonant oscillator when it was over three times above threshold.³¹ The losses of the OPO cavity mirrors and the crystal surfaces gave a total round-trip loss at the signal wavelength of $\sim 7\%$.

At maximum pumping (300-W peak power, five times above threshold), the OPO ran robustly, with a pump depletion of 43% as shown in Fig. 15. The OPO threshold was measured to be 60 W peak. By adjusting the width of the square pulse with the acousto-optic modulator, we could vary the OPO pulse duration over 150–600 ns. The OPO could be operated over 0–9 kHz. A maximum signal-pulse energy of 5 μJ was recorded with a pump pulse of 52 μJ (1-kHz repetition rate). Lower-loss coatings on the OPO cavity mirrors and the PPLN crystal would significantly reduce the oscillation threshold and increase the in-the-bucket conversion efficiency.

The saturated pump depletion level is ~ 26 W, shown as the flat part of the depleted pump pulse in Fig. 15. This steady-state value is a measure of the threshold for cw SRO operation. The threshold for a cw SRO operating in the near field is given by⁴

$$P_{\text{th}} = \frac{n_p n_s n_i \epsilon_0 c^3 \pi (w_p^2 + w_s^2)}{4 \omega_s \omega_i d_Q^2 L^2} a_s, \quad (13)$$

where a_s is the round-trip signal power loss, including output coupling, and $w_p = 47$ μm and $w_s = 63$ μm are the Gaussian mode waists at the pump and the signal, respectively. Because the Gaussian mode sizes expand by $<15\%$ through the crystal, the near-field approximation is applicable. The nonlinear coefficient is $d_Q = 14.4$ pm/V, where d_{eff} has been adjusted for constant Miller delta as before. The calculated threshold of 23 W is in good agreement with the value obtained from saturated pump depletion. These pump levels are within the reach of current single-mode cw Nd:YAG lasers, offering the potential for a useful high-power cw tunable mid-IR source.

We measured the linewidth of the OPO by looking at the transmission of its output through solid étalons 0.27, 1.5, and 7 mm thick. Depending on the spacing

between the cavity mirrors and the PPLN crystal, the linewidth of the OPO varied from single longitudinal mode (<0.5 GHz) to 360 GHz. Intracavity étalon effects are likely responsible for the very narrow-linewidth operation; our research shows that even a very weak étalon (finesse <1) is effective in limiting the linewidth of a low-gain OPO. We expect that reducing the linewidth of this OPO will be much easier than for conventional 10–50-ns OPO's.³² Use of weak étalons, or perhaps just increasing the OPO rise time by tailoring the pump laser pulse with the acousto-optic modulator, will yield narrow linewidths without the complexity associated with other techniques such as grazing-incidence grating cavities³³ and injection seeding.³⁴

In summary, this long-pulse OPO is a novel device that permits significant control over its temporal pulse duration and shape. This device may prove advantageous for reducing the intrinsic linewidth of simple, two-mirror cavity OPO's and has shown that moderate threshold cw singly resonant OPO's are possible with PPLN.

C. Cw-Diode-Pumped PPLN OPO

For doubly resonant oscillators (DRO's) in PPLN, calculations predict thresholds readily within range of commercially available cw diode lasers. An OPO directly pumped by a diode laser is especially interesting as a compact and efficient source of tunable radiation. Previous attempts to build a diode-pumped OPO with available nonlinear optical materials have been hampered because the gain and phase-matching conditions placed difficult constraints on the wavelength and power requirements of the pump laser.³⁵ With the engineerable phase matching and high-gain properties available through quasi-phase matching, we recently demonstrated an OPO directly pumped by a commercial cw diode laser.³⁶

The experimental setup of the diode-pumped OPO is shown in Fig. 16. The pump was a 977.6-nm master-oscillator–power-amplifier diode laser from SDL, Inc. (Model 5762), operated at 500 mW. We used a scanning confocal interferometer to verify single-frequency operation of the diode laser; the laser linewidth was ~ 25 MHz. The laser was susceptible to even small amounts of feedback, and -60 -dB isolation was required

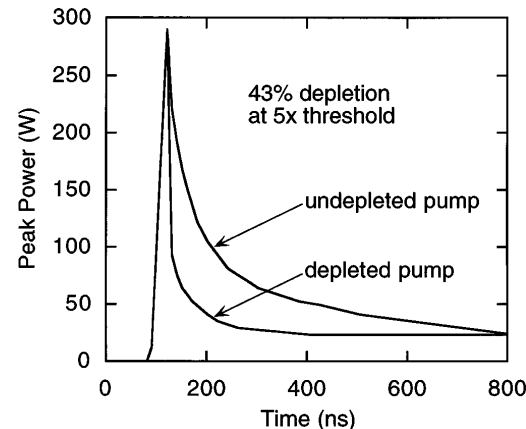


Fig. 15. Pump pulse transmitted through the long-pulse OPO cavity with the OPO off (upper trace) and the OPO on (lower trace). The OPO turns on after 30 ns, and the transmitted pump quickly saturates to ~ 26 W, the oscillation threshold.

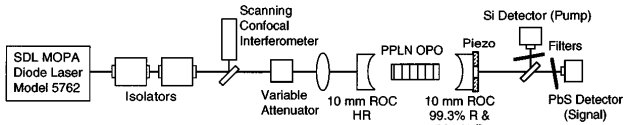


Fig. 16. Experimental setup for a diode-pumped OPO in bulk PPLN: ROC, radius of curvature; HR, highly reflecting; R, reflecting.

for stable operation. The DRO resonator was a linear cavity with 10-mm radius-of-curvature mirrors separated by 22 mm. We used a high-reflectivity input mirror and output couplers of 0.3% and 0.7% transmission, all centered at 1.96 μm . The useful bandwidth of the mirrors was $\sim 200 \text{ nm}$, and the pump reflectivity was $\sim 20\%$. The pump beam was focused to a 33- μm waist in the cavity, with a beam quality of $M^2 = 1.3$. The output coupler was mounted upon an annular piezoelectric element (piezo) for cavity length control. The OPO output near 1.96 μm was detected with a PbS detector after a filter that blocked the pump beam, while the transmitted pump beam was detected with a Si detector.

The PPLN crystal for the diode-pumped OPO was 0.5 mm thick with a 9.3-mm interaction length. The domain period for quasi-phase matching was 28.5 μm , designed for degenerate operation at 88 $^\circ\text{C}$, as shown in Fig. 17. The polished end faces of the PPLN were AR coated for the signal–idler pair near degeneracy. The total single-pass power loss through the two coated surfaces and the crystal was 0.8% at 2.014 μm , as described in Section 3. The peak phase-matching temperature was measured at 91 $^\circ\text{C}$, which agrees with the design calculation.

Figure 18 shows the cavity-mirror piezo voltage, the pump transmission through the cavity, and the OPO output through a 0.7% output coupler as the cavity length was scanned with the piezo. Note where the piezo position was held at a resonant point for the OPO during the flat part before the voltage ramp. The relatively stable nature of the output at this point indicates the potential for adding control electronics to make a useful cw infrared tunable source. The OPO output could be shifted relative to the pump transmission by adjustment of the temperature and the cavity length. The upper plot in Fig. 18 shows a case in which the output occurs near a peak of the pump transmission, and the lower plot shows a different operating point where the OPO output occurs near a pump transmission minimum. The 20% reflectivity of the cavity mirrors at the pump wavelength formed a cavity with finesse of 1.7, so the circulating pump intensity could range from 0.5 to 1.2 times the incident power. Even a low-finesse cavity such as this can produce noticeable étalon effects, but the fact that the OPO oscillated during the pump transmission minimum indicates that threshold was reached without pump enhancement.

The threshold for a DRO near degeneracy is given by⁴

$$P_{\text{th}} = \frac{a_s a_i n_s n_i c^4 \epsilon_0 \pi}{4 \omega_s \omega_i \omega_p d_Q^2 L \bar{h}_m}, \quad (14)$$

where \bar{h}_m is the Boyd–Kleinman reduction factor³⁷ for a focused interaction and a_s and a_i are the round-trip power

losses at the signal and the idler, respectively. The nonlinear coefficient is $d_Q = 13.2 \text{ pm/V}$, again after adjustment for constant Miller delta. The round-trip power losses for the signal and the idler were 1.9% and 2.3% for the 0.3% and 0.7% output couplers, respectively. Minimum threshold is attained when $L/b = 2.8$ and $\bar{h}_m = 1.07$. In our case, $\bar{h}_m \approx L/b = 0.62$ (the waists are $w_p = 33 \mu\text{m}$ and $w_s = 47 \mu\text{m}$). The predicted threshold power was

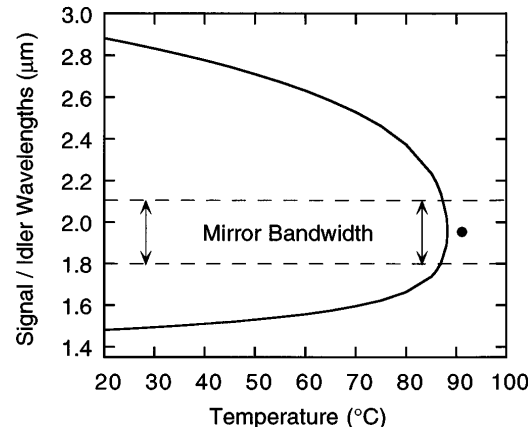


Fig. 17. Calculated temperature tuning curve for 977.6-nm-pumped, 28.5- μm -period PPLN OPO. The calculated phase-matching temperature at degeneracy is 88 $^\circ\text{C}$; the experimental measurement is 91 $^\circ\text{C}$. The bandwidth of the mirrors used in the diode-pumped OPO experiment is indicated.

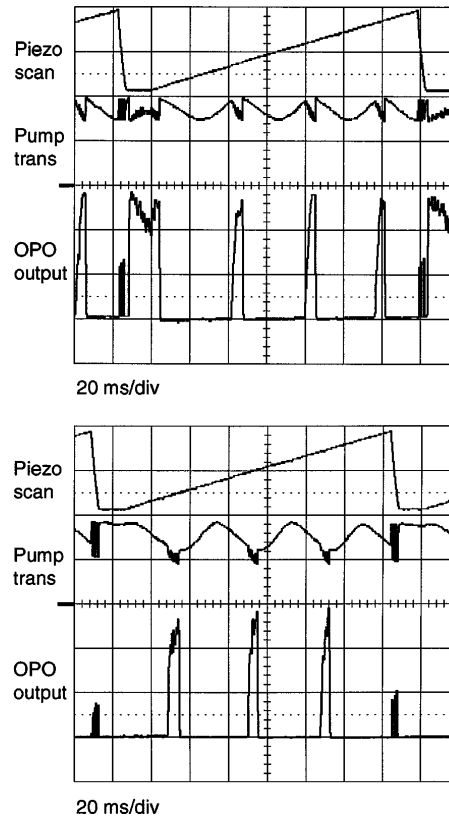


Fig. 18. Cavity-mirror piezo scan voltage, pump transmission with depletion, and $\sim 1.96\text{-}\mu\text{m}$ OPO output signals with a 0.7% output coupler. The upper plot shows an operating point near the peak of the pump transmission. The lower plot shows a different operating point near the minimum of the pump transmission.

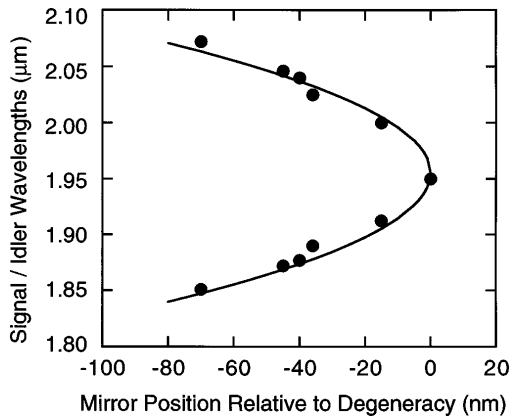


Fig. 19. Centroid of the spectral output of the cw diode-pumped DRO as a function of cavity-mirror separation.

52 and 76 mW for the 0.3% and 0.7% output couplers, respectively; the measured thresholds were 61 and 98 mW.

The OPO runs in disjoint regions as a function of cavity-mirror separation because of the cluster effect that is well-known for DRO's.³⁸ As one can see by examining the pump resonance in Fig. 18, the cluster spacing is half the pump wavelength, or 489 nm. We monitored the spectral content of the OPO output, using a 1-m monochromator. For different wavelength settings we observed the monochromator output while the cavity mirror was scanned. The output spectrum was erratic because of lack of cavity stabilization, but the centroid of the monochromator output showed a clear dependence on the cavity-mirror separation, which is plotted in Fig. 19. With a mirror translation of 70 nm, signal-idler pairs were observed from 1.85 to 2.08 μm, matching the mirror bandwidths. As the cavity length is scanned, the output frequencies follow the cavity resonance until they reach degeneracy. There is a subsequent gap in the OPO output until the cavity length changes enough to bring another cluster within the mirror bandwidths.

For 370 mW of pump incident upon the cavity mirror, we measured peak output powers of 34 and 64 mW with 0.3% and 0.7% output couplers, respectively. The conversion efficiencies of 9% and 17% agree with the values obtained from pump depletion. The theoretical conversion efficiency is given by⁴

$$\frac{P_s + P_i}{P_p} = 2 \frac{T_{oc}}{T_{oc} + a_d} \frac{\sqrt{N} - 1}{N}, \quad (15)$$

where T_{oc} is the transmission of the output coupler, a_d is the combined loss in the crystal and in the other cavity mirror, and N is the number of times above threshold. Using our measured threshold values gives predicted efficiencies of 8% and 15% for the 0.3% and 0.7% output couplers, respectively.

In summary, we have demonstrated a cw diode-pumped DRO with PPLN. The high-gain and engineerable phase-matching properties of PPLN permit tailoring the material to match commercially available diode lasers. The fact that the output could be made to run continuously indicates the potential for stabilizing the OPO power with servo control of the cavity length. With this addition and by incorporating vibration and environmental isolation, we expect to see the spectral behavior improve.

5. FUTURE RESEARCH EFFORTS

SRO's are generally preferable to DRO's because they are more stable and tuning is better behaved; however, their high thresholds have made cw SRO's difficult to build.³⁹ The high gain of d_{33} interactions in PPLN makes possible a widely tunable cw SRO with modest pump power. When we use the expression given in Eq. (13), the calculated threshold of a 1.064-μm pumped cw SRO is ~3 W for confocal focusing ($w_{op} = 34$ μm, $w_{os} = 41$ μm) in a 15-mm-long PPLN crystal with 2% round-trip power loss at the signal ($\lambda_s = 1.54$ μm). Although the near-field expression loses accuracy for a confocal resonator, the calculation gives an indication that cw SRO operation can be reached at a power level that is currently available in single-transverse-mode Nd:YAG lasers. The high average power in the proposed cw SRO will cause no problem because the absorption in PPLN is low, as demonstrated by a previous resonant SHG experiment (65 W of circulating 1.064-μm cw power with a 15-μm waist).²⁶ We expect to operate a cw SRO by using a diode-pumped Nd:YAG laser in the near future.⁴⁰ High-energy-power pulsed OPO's are also of interest. Commercial Q-switched diode-pumped Nd:YAG lasers operating at ~10 kHz are capable of driving compact, efficient OPO's generating output at the watt level.

Photorefractive damage in PPLN is a factor of concern in the push to high-average-power operation. Although the erasure of photorefractive damage that we showed in Subsection 4.A is acceptable in many situations, there are alternatives that might permit high-average-power operation at room temperature. We can manipulate the grating design to minimize the processes that drive photorefractive damage. The effect of a change in either the grating period or the duty cycle on the phase matching is in proportion to the coherence length. Because the coherence lengths of visible interactions are much smaller than those in the infrared, a small change in grating pattern can have a large effect on the visible while having a negligible effect on the infrared. Hence one can use a perturbation of the duty cycle or the period to minimize green generation, which is the primary contributor to photorefractive damage in a 1-μm-pumped OPO, while maintaining the average grating period and duty cycle needed for efficient infrared generation. Although either the duty cycle or the period can readily be altered on the lithographic mask, the grating period may be the easiest factor to control because poled material shows less variation in this parameter relative to the pattern on the mask. Another approach for reduction of the photorefractive effect is to start with a more damage-resistant material such as LiTaO₃ or MgO:LiNbO₃. Both are structurally similar to LiNbO₃. Periodically poled LiTaO₃ was successfully fabricated with the electric-field poling technique, and presumably MgO:LiNbO₃ can be periodically poled as well.¹⁷

An area of active research to reduce OPO thresholds further is the use of waveguides. A waveguide OPO in PPLN has been demonstrated with periodic poling that was fabricated by the Ti-indiffusion technique.¹² This approach yields domain-inverted regions that are triangular in depth, causing a reduction in efficiency compared with those of the ideal vertical domains of electric-field

poled PPLN. The problem of optimizing devices is compounded by the depth-dependent overlap between the waveguide modes and the domain grating. Electric-field poled PPLN is expected to improve the device significantly, and an optimized waveguide OPO that uses it is predicted to have a cw SRO threshold below 100 mW, making it suitable for pumping by a single-stripe diode laser.⁴¹

The flexibility of engineering phase matching through the QPM grating opens up a fertile design space. We mentioned above the potential for multiwavelength operation and broadband phase matching. The first intended extension of QPM design in our OPO's will be a tunable grating device. SHG with a fanned grating has been used to match various diode-laser wavelengths in PPLN waveguides.⁴² In a QPM OPO a fanned grating would permit tuning the device by translation of the crystal transversely through the beam so that the beam interacts with different grating periods at different positions. Suitable design will permit continuous tuning over the entire mid-infrared range of LiNbO₃ with a simple translation of the crystal by <10 mm.

The broad phase-matching bandwidth that permits the desirable wide tunability of PPLN OPO's is an asset for wideband amplification; however, for many applications, narrow-band operation may be required. Line narrowing techniques employed in conventional OPO's, such as grazing-incidence gratings and injection seeding, can be applied to QPM OPO's as well. We have noted in Subsection 4.B that long-pulse operation, for which the high nonlinear drive of PPLN is helpful, may offer a simple scheme of linewidth narrowing. A promising approach to making a low-power narrow-band oscillator is with a TIR monolithic resonator design.^{23,43} Stability provided by the monolithic resonator combined with a clean single-frequency solid-state pump laser, such as a nonplanar ring oscillator, leads to stable single-frequency OPO output. Type-I phase matching was used for such devices in the past because it is the only interaction accessible with birefringent phase matching in LiNbO₃. However, with both the signal and the idler having the same polarization, their coupling to the resonator cannot be separately controlled, and double-resonance effects that impair stability and limit tunability are unavoidable. Critical birefringent phase-matching designs also suffer from Poynting-vector walk-off, which raises the threshold. We propose to build a 1.064-μm-pumped LiNbO₃ monolithic TIR OPO with a noncritically phase-matched QPM section in one leg. We plan to use Type-II phase matching so that the signal and the idler can be separately controlled with birefringent elements and because the bandwidth is inherently narrower (see Table 2). Type-II phase matching in LiNbO₃ is readily implemented by use of quasi-phase matching with domain periods of ~14 μm that are within our present PPLN fabrication capabilities.

6. CONCLUSION

Quasi-phase matching permits engineering OPO performance for a variety of configurations. Standard OPO theory applies to QPM OPO's with simple substitutions for effective nonlinear coefficient and wave-vector mismatch. A QPM OPO can be noncritically phase matched

with no walk-off at a given temperature for any collinear interaction within the transparency range of the material. High gain is available with the large diagonal nonlinear coefficient.

PPLN is now available as a bulk nonlinear optical crystal for QPM OPO's. The electric-field poling technique is a onetime permanent process that lends itself to commercial manufacturing. PPLN has parametric gain ~20 times higher than single-domain LiNbO₃, with no additional loss or damage susceptibility. With our fabrication methods we regularly obtain device-quality PPLN samples more than 15 mm long with apertures of 15 mm × 0.5 mm. Demonstrated periods of >10 μm cover the important infrared interactions. Continued process development will lead to pieces 5 cm long and 1 mm thick.

We have demonstrated what is to our knowledge the first bulk QPM OPO by using PPLN. Rapid progress in material development has led to variety of OPO devices:

- Short-pulse (~10-ns) SRO's pumped by Q-switched 1.064-μm Nd:YAG lasers with thresholds as low as 12 μJ, 70% pump conversion, no damage at ~10 times above threshold, high-average-power pumping (1 W_{av} at 10 kHz), and tunable output from 1.45 to 4 μm.
- A long-pulse SRO (~500 ns) pumped by a 1.064-μm Nd:YAG laser, with threshold at 60-W peak power, indicating the potential for a cw SRO threshold of ~10 W.
- A cw DRO directly pumped by a commercial 978-nm cw diode laser with thresholds below 80 mW and outputs above 60 mW at 1.96 μm.

This research shows the potential for QPM OPO's to become practical devices with currently available pump lasers. PPLN promises to be an important material for applications requiring sources in the range 1 to >4 μm.

*Present address, U.S. Air Force Wright Laboratory, WL/AARI-2, Wright-Patterson AFB, Ohio 45433.

ACKNOWLEDGMENTS

We thank G. D. Miller for collaboration during the development of the electric-field poling process, M. L. Bortz for performing measurements of difference-frequency generation, and Crystal Technology, Inc., for supplying LiNbO₃ wafers. This research was supported by the U.S. Office of Naval Research, the U. S. Air Force Phillips Laboratory, the U. S. Air Force Wright Laboratory, the Stanford Office of Technology Licensing, and the Advanced Research Projects Agency through the Center for Nonlinear Optical Materials at Stanford University.

REFERENCES

1. M. M. Fejer, G. A. Magel, D. H. Jundt, and R. L. Byer, "Quasi-phase-matched second harmonic generation: tuning and tolerances," *IEEE J. Quantum Electron.* **28**, 2631–2654 (1992).
2. M. Yamada, N. Nada, M. Saitoh, and K. Watanabe, "First-order quasi-phase matched LiNbO₃ waveguide periodically poled by applying an external field for efficient blue second-harmonic generation," *Appl. Phys. Lett.* **62**, 435–436 (1993).
3. W. K. Burns, W. McElhanon, and L. Goldberg, "Second harmonic generation in field poled, quasi-phase-matched, bulk LiNbO₃," *IEEE Photon. Technol. Lett.* **6**, 252–254 (1994).

4. R. L. Byer, "Optical parametric oscillators," in *Quantum Electronics: A Treatise*, H. Rabin and C. L. Tang, eds. (Academic, New York, 1975), pp. 587–702.
5. G. J. Edwards and M. Lawrence, "A temperature-dependent dispersion equation for congruently grown lithium niobate," *Opt. Quantum Electron.* **16**, 373–374 (1984).
6. Y. S. Kim and R. T. Smith, "Thermal expansion of lithium tantalate and lithium niobate single crystals," *J. Appl. Phys.* **40**, 4637–4641 (1969).
7. D. A. Roberts, "Simplified characterization of uniaxial and biaxial nonlinear optical crystals: a plea for standardization of nomenclature and conventions," *IEEE J. Quantum Electron.* **28**, 2057–2074 (1992).
8. M. L. Bortz, D. Serkland, and M. M. Fejer, "Near degenerate difference frequency generation at 1.3 μm in LiNbO₃ waveguides for application as an all-optical channel shifter," in *Conference on Lasers and Electro-Optics*, Vol. 8 of 1994 OSA Technical Digest Series (Optical Society of America, Washington, D.C., 1994), pp. 288–289.
9. M. L. Bortz, M. Fujimura, and M. M. Fejer, "Increased acceptance bandwidth for quasi-phase-matched second harmonic generation in LiNbO₃ waveguides," *Electron. Lett.* **30**, 34–35 (1994).
10. J. A. Armstrong, N. Bloembergen, J. Ducuing, and P. S. Pershan, "Interactions between light waves in a nonlinear dielectric," *Phys. Rev.* **127**, 1918–1939 (1962).
11. E. J. Lim, M. M. Fejer, and R. L. Byer, "Second harmonic generation of green light in periodically poled planar lithium niobate waveguide," *Electron. Lett.* **25**, 174–175 (1989).
12. M. L. Bortz, M. A. Arbore, and M. M. Fejer, "Quasi-phase-matched optical parametric amplification and oscillation in periodically poled LiNbO₃ waveguides," *Opt. Lett.* **20**, 49–51 (1995).
13. G. A. Magel, M. M. Fejer, and R. L. Byer, "Quasi-phase-matched second harmonic generation of blue light in periodically poled LiNbO₃," *Appl. Phys. Lett.* **56**, 108–110 (1990).
14. Y. Lu, L. Mao, and N. Ming, "Blue-light generation by frequency doubling of an 810-nm cw GaAlAs diode laser in a quasi-phase-matched LiNbO₃ crystal," *Opt. Lett.* **19**, 1037 (1994).
15. H. Ito, C. Takyu, and H. Inaba, "Fabrication of periodic domain grating in LiNbO₃ by electron beam writing for application of nonlinear optical processes," *Electron. Lett.* **27**, 1221–1222 (1991).
16. J. Webjörn, V. Pruner, P. St. J. Russell, J. R. M. Barr, and D. C. Hanna, "Quasi-phase-matched blue light generation in bulk lithium niobate, electrically poled via periodic liquid electrodes," *Electron. Lett.* **30**, 894–895 (1994).
17. S. N. Zhu, Y. Y. Zhu, Z. Y. Zhang, H. Shu, H. F. Wang, J. F. Hong, C. Z. Ge, and N. B. Ming, "LiTaO₃ crystal periodically poled by applying an external pulsed field," *J. Appl. Phys.* **77**, 5481–5483 (1995).
18. Q. Chen and W. P. Risk, "Periodic poling of KTiOPO₄ using an applied electric field," *Electron. Lett.* **30**, 1516–1517 (1994).
19. L. E. Myers, G. D. Miller, R. C. Eckardt, M. M. Fejer, R. L. Byer, and W. R. Bosenberg, "Quasi-phase-matched 1.064- μm -pumped optical parametric oscillator in bulk periodically poled LiNbO₃," *Opt. Lett.* **20**, 52–54 (1995).
20. L. E. Myers, R. C. Eckardt, M. M. Fejer, and R. L. Byer, "Quasi-phase-matched optical parametric oscillators using bulk periodically poled LiNbO₃," in *Solid State Lasers and Nonlinear Crystals*, G. J. Quarles, L. Esterowitz, and L. K. Cheng, eds., *Proc. Soc. Photo-Opt. Instrum. Eng.* **2379**, 154–162 (1995).
21. A. Räuber, "Chemistry and physics of lithium niobate," in *Current Topics in Materials Science*, E. Kaldis, ed. (North-Holland, Amsterdam, 1978), p. 503.
22. I. Camlibel, "Spontaneous polarization measurements in several ferroelectric oxides using a pulsed-field method," *J. Appl. Phys.* **40**, 1690–1693 (1969).
23. D. K. Serkland, R. C. Eckardt, and R. L. Byer, "Continuous-wave total-internal-reflection optical parametric oscillator pumped at 1.064 nm," *Opt. Lett.* **19**, 1046–1048 (1994).
24. S. J. Brosnan and R. L. Byer, "Optical parametric oscillator threshold and linewidth studies," *IEEE J. Quantum Electron.* **QE-15**, 415–431 (1979).
25. M. M. Choy and R. L. Byer, "Accurate second-order susceptibility measurements of visible and infrared nonlinear crystals," *Phys. Rev. B* **14**, 1693–1706 (1976).
26. D. H. Jundt, G. A. Magel, M. M. Fejer, and R. L. Byer, "Periodically poled LiNbO₃ for high-efficiency second-harmonic generation," *Appl. Phys. Lett.* **59**, 2657–2659 (1991).
27. A. Ashkin, G. D. Boyd, J. M. Dziedzic, R. G. Smith, A. A. Ballman, J. J. Levenstein, and K. Nassau, "Optically induced refractive index inhomogeneities in LiNbO₃ and LiTaO₃," *Appl. Phys. Lett.* **9**, 72–74 (1966).
28. W. R. Bosenberg, A. Drobshoff, D. C. Gerstenberger, L. E. Myers, R. C. Eckardt, M. M. Fejer, and R. L. Byer, "Long pulse optical parametric oscillator based on bulk periodically poled LiNbO₃," in *Advanced Solid State Lasers*, Addendum to 1995 OSA Technical Digest Series (Optical Society of America, Washington, D.C., 1995), postdeadline paper PD8.
29. See previous features on OPO's: *J. Opt. Soc. Am. B* **10**, 1656–1790, 2148–2243 (1993).
30. H. Plaessmann, S. A. Re, J. J. Alonis, D. L. Vecht, and W. M. Grossman, "Multipass diode-pumped solid-state optical amplifier," *Opt. Lett.* **18**, 1420–1422 (1993).
31. S. T. Yang, R. C. Eckardt, and R. L. Byer, "Power and spectral characteristics of continuous-wave parametric oscillators: the doubly to singly resonant transition," *J. Opt. Soc. Am. B* **10**, 1684–1695 (1993).
32. W. J. Kozlovsky, E. K. Gustafson, R. C. Eckardt, and R. L. Byer, "Efficient monolithic MgO:LiNbO₃ singly resonant optical parametric oscillator," *Opt. Lett.* **13**, 1102–1104 (1988).
33. W. R. Bosenberg and D. R. Guyer, "Single frequency optical parametric oscillator," *Appl. Phys. Lett.* **61**, 387–389 (1992).
34. J. E. Bjorkholm and H. G. Danielmeyer, "Frequency control of a pulsed optical parametric oscillator by radiation injection," *Appl. Phys. Lett.* **15**, 171–173 (1969).
35. See M. Scheidt, B. Beier, R. Knappe, K. J. Boller, and R. Wallenstein, "Diode-laser-pumped continuous-wave KTP optical parametric oscillator," *J. Opt. Soc. Am. B* **12**, 2087–2094 (1995).
36. L. E. Myers, R. C. Eckardt, M. M. Fejer, R. L. Byer, J. W. Pierce, and R. G. Beausoleil, "CW diode-pumped optical parametric oscillator in bulk periodically poled LiNbO₃," in *Advanced Solid State Lasers*, Addendum to 1995 OSA Technical Digest Series (Optical Society of America, Washington, D.C., 1995), postdeadline paper PD9.
37. G. D. Boyd and D. A. Kleinman, "Parametric interaction of focused Gaussian light beams," *J. Appl. Phys.* **39**, 3596–3639 (1968).
38. J. A. Giordmaine and R. C. Miller, "Optical parametric oscillation in the visible spectrum," *Appl. Phys. Lett.* **9**, 298–300 (1966).
39. S. T. Yang, R. C. Eckardt, and R. L. Byer, "Continuous-wave singly resonant optical parametric oscillator pumped by a single-frequency resonantly doubled Nd:YAG laser," *Opt. Lett.* **18**, 971–973 (1993).
40. R. J. Shine, A. J. Alfrey, and R. L. Byer, "40-W cw, TEM₀₀-mode, diode-laser-pumped, Nd:YAG miniature-slab laser," *Opt. Lett.* **20**, 459–461 (1995).
41. M. A. Arbore, M. L. Bortz, and M. M. Fejer, "Quasi-phase-matched optical parametric oscillators in lithium niobate waveguides as sources of widely tunable infrared coherent radiation," in *Nonlinear Guided Waves and Their Applications*, Vol. 6 of 1995 OSA Technical Digest Series (Optical Society of America, Washington, D.C., 1995), pp. 162–164.
42. Y. Ishigame, T. Suhara, and H. Nishihara, "LiNbO₃ waveguide second-harmonic-generation device phase matched with a fan-out domain-inverted grating," *Opt. Lett.* **16**, 375–377 (1991).
43. S. Schiller and R. L. Byer, "Quadruply resonant optical parametric oscillation in a monolithic total-internal-reflection resonator," *J. Opt. Soc. Am. B* **10**, 1696–1707 (1993).